

Chaos Beyond Linearized Stability Analysis: Folding of the Phase Space and Distribution of Lyapunov Exponents

P. G. Silvestrov¹ and I. V. Ponomarev²

¹Instituut-Lorentz, Universiteit Leiden, P.O. Box 9506, 2300 RA Leiden, The Netherlands

²Queens College of the City University of New York, Flushing, NY 11367

(Dated: 26 September 2004)

We have found a universal mechanism which leads to the enhanced probability, $P(\lambda, t)$, to find small values of the finite time Lyapunov exponent, λ . In our investigation of chaotic dynamical systems we go beyond the linearized stability analysis of nearby divergent trajectories and consider folding of the phase space in the course of chaotic evolution. We show that the spectrum of the Lyapunov exponents $F(\lambda) = \lim_{t \rightarrow \infty} t^{-1} \ln P(\lambda, t)$ at the origin has a finite value $F(0) = -\tilde{\lambda}$ and a slope $F'(0) \leq 1$. This means that all negative moments of the distribution $\langle e^{-m\lambda t} \rangle$ are saturated by rare events with $\lambda \rightarrow 0$. Extensive numerical simulations confirm our findings.

PACS numbers: 05.45.-a, 05.45.Ac, 02.70.Rr, 05.45.Mt

An exponential divergency of nearby trajectories is commonly considered as a paradigm of classical chaos [1, 2]. The mathematical structure behind this divergency appears to be rather simple. The time evolution of the distance in phase space between two trajectories is determined by the monodromy matrix $\mathcal{M}(t)$, whose largest eigenvalue grows exponentially like $e^{\lambda t}$, with λ being the Lyapunov exponent. An evolution of small areas in phase space in this linearized approximation may always be described by a combination of area preserving stretching and squeezing (we assume two canonical variables x and p). In spite of a broad literature in the field we are not aware of results going beyond the linearized stability analysis of dynamics of close trajectories. In this letter we try to fill this gap and consider the effect of bending of phase space on the probability distribution of finite-time Lyapunov exponents $P(\lambda, t)$ [2, 3, 4, 5]. Knowing this distribution is important for many applications, ranging from the problems of ocean acoustics [6] and branching of 2d electron flow [7] to mesoscopic superconductivity [8, 9, 10]. As we will see, a creation of narrow folds in the course of mapping of the phase plane results in a great enhancement of the probability to find small values of λ . As a result all the negative moments $\langle e^{-m\lambda t} \rangle$ for sufficiently large times t are saturated by the rare events with $\lambda \rightarrow 0$.

For large times the distribution of Lyapunov exponents has a generic form [2] ($\lambda \geq 0$)

$$P(\lambda, t) \approx \sqrt{t/\lambda_2} \exp[tF(\lambda)], \quad (1)$$

with a model specific function $F(\lambda)$ called spectrum [3]. The conventional selfaveraging Lyapunov exponent λ_0 appears in the expansion of spectrum around the maximum $F \approx -(\lambda - \lambda_0)^2/2\lambda_2$. If the evolution of the system is described by a Markovian process, i.e. if $P(\lambda, t)$ for large t is given by a convolution of $P(\lambda, t_i)$ for smaller time intervals, then naturally $F(0) = -\infty$. On the other hand, the limit of mixed phase space has $F(0) = 0$ [3]. We argue that in the case of fully developed dynamical chaos the spectrum still has a finite limit

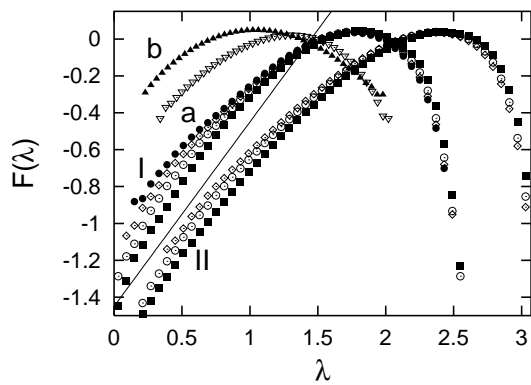


FIG. 1: The spectrum $F(\lambda) = \ln(P(\lambda, t))/t$ for the kicked rotator for different kicking strengths $K = 11$ (I) and $K = 20$ (II), and times $t = 10(\blacksquare)$, $15(\circ)$, $20(\diamond)$, $25(\bullet)$, and for the time dependent random potential for two regimes $a(\nabla)$ and $b(\blacktriangle)$ described in the text. In case b due to the small values of Lyapunov exponent both $F(\lambda)$ and λ were multiplied by 5. The solid line shows a slope $F'(\lambda) = 1$.

$$F(0) = \text{const} < 0.$$

Dynamics of close trajectories is determined by the monodromy matrix via

$$\begin{pmatrix} \delta p \\ \delta x \end{pmatrix} = \mathcal{M} \begin{pmatrix} \delta p_0 \\ \delta x_0 \end{pmatrix}; \mathcal{M} = \begin{pmatrix} \frac{\partial p}{\partial p_0} & \frac{\partial p}{\partial x_0} \\ \frac{\partial x}{\partial p_0} & \frac{\partial x}{\partial x_0} \end{pmatrix}. \quad (2)$$

The Lyapunov exponent is defined as [11]

$$\lambda = (2t)^{-1} \ln \left[\text{tr} \mathcal{M}^T \mathcal{M} / 2 + \sqrt{(\text{tr} \mathcal{M}^T \mathcal{M} / 2)^2 - 1} \right]. \quad (3)$$

Before presenting our analytical theory, we show in Fig. 1 the spectrum $F(\lambda) = \ln(P(\lambda, t))/t$, found numerically for two models. The first model, which we will mostly use hereafter, is the kicked rotator [1]:

$$\begin{aligned} p_{n+1} &= p_n + K \sin x_n, \\ x_{n+1} &= x_n + p_{n+1}. \end{aligned} \quad (4)$$

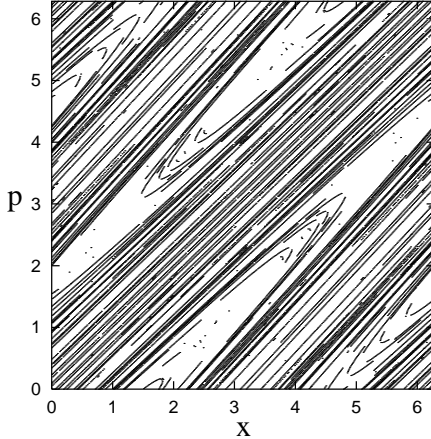


FIG. 2: Distribution of the endpoints of trajectories (x_t, p_t) having a small value of Lyapunov exponent $\lambda < \lambda_0/18$, $\lambda_0 = \ln(K/2)$ for the kicked rotator with $K = 20$ after 5 iterations.

The spectrum $F(\lambda)$ in Eq. (1) is strictly defined in the limit $t \rightarrow \infty$. Due to a vanishing probability $P(\lambda = 0, t) \equiv 0$ finite time approximations always have $F_t(0) = -\infty$, but this singularity becomes weaker with time increased. This tendency can be observed in Fig. 1, where different finite time plots are presented (see especially the case for $K = 11$).

The second model describes a particle moving under the action of time dependent random force, which we introduced via the “random kick” Hamiltonian

$$H = \frac{p^2}{2} + \kappa \sum_n \delta(t-n) \sum_{q=1}^N (a_q^{(n)} \sin qx + b_q^{(n)} \cos qx). \quad (5)$$

Here the random coefficients $-1 < a_q^{(n)}, b_q^{(n)} < 1$. Both plots in Fig. 1 are for $\kappa = 1$: the first one (a) has $N = 3$ and 50 random kicks, while the second plot (b) has $N = 1$ and 300 kicks. The behavior of the spectrum for large λ is completely different for two models. However, a shape of the left wing of $F(\lambda)$ appears to be surprisingly similar. The results of all simulations are consistent with a linear increase at $\lambda \ll \lambda_0$, i.e. $F(0) = \text{const}, F'(0) = 1$.

The distribution of Lyapunov exponents, Eq. (1), is a rough statistical characteristic which ignores correlations of values of λ between different trajectories. Such correlations are seen in Fig. 2, where we show the position on the phase plane of the endpoints of trajectories having a small value of λ . The points on the figure are not distributed uniformly, but concentrate into a narrow lines. A formation of such structures is explained in Fig. 3. The figure shows a time evolution of a small area of initial points x_0, p_0 on the phase plane surrounding some classical trajectory $p(\tau), x(\tau)$. The evolution of the area is conveniently described by the transformation of a small piece of square lattice covering this area (Fig. 3a). Few stages of such an evolution are shown.

The first stage, shown in Fig. 3b consists of linear extension and squeezing. For the appropriate orientation

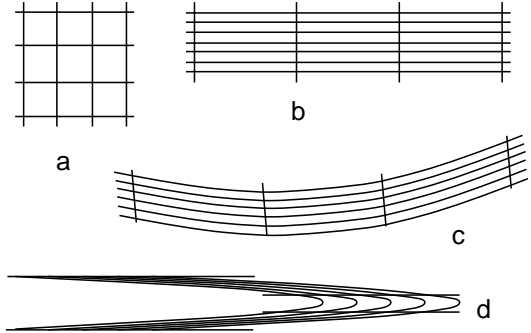


FIG. 3: Schematic presentation of the evolution of a small phase space area, see description in the text. The stages **b-d** correspond to different orientations of the original frame **a**.

of initial and final axes it may be expressed as

$$u \rightarrow ue^{\lambda_0 t_1}, \quad v \rightarrow ve^{-\lambda_0 t_1}. \quad (6)$$

At this moment we forget about the fluctuations of the Lyapunov exponents and use λ_0 for estimates. The linear transformation (6) always describes the evolution of infinitesimally small areas. For small but finite regions of phase space a nonlinear term should be added to Eq. (6)

$$u \rightarrow u, \quad v \rightarrow v + u^2/2, \quad (7)$$

which is shown in Fig. 3c. Parabolas in Fig. 3c have a curvature comparable to the size of the system, or the typical momentum, both assumed to be of the order unity. A consequent evolution of the area consists of further stretching and squeezing. It is important that the map, built from straight lines and parabolas shown in Fig. 3c, is robust under such a transformation. Squeezing of a parabola gives another parabola (generically more narrow due to chaos). It is shown in Fig. 3d and may be expressed as

$$u \rightarrow ue^{-\lambda_0 t_2}, \quad v \rightarrow ve^{\lambda_0 t_2}. \quad (8)$$

This last squeezing leads to diminishing of the exponential divergency and formation of a stripe with small values of λ along the center of narrow parabolas in Fig. 3d. These stripes appear as narrow black lines in Fig. 2. Combining together eqs. (6-8) we express new coordinates u and v through initial ones u_0 and v_0

$$u = u_0 e^{\lambda_0(t_1-t_2)}, \quad v = v_0 e^{\lambda_0(t_2-t_1)} + \frac{u_0^2}{2} e^{\lambda_0(t_2+2t_1)}. \quad (9)$$

Now the Lyapunov exponent is calculated with the help of the monodromy matrix \mathcal{M} via $\lambda \approx \ln \mathcal{M}_{ij}^2/2t$:

$$\lambda = \frac{1}{2t} \ln \left[2\text{ch}(2\lambda_0(t_1 - t_2)) + u^2 e^{2\lambda_0(t_2+t)} \right], \quad (10)$$

where $t = t_1 + t_2$. Thus the finite time Lyapunov exponent depends only on one variable u . This explains the

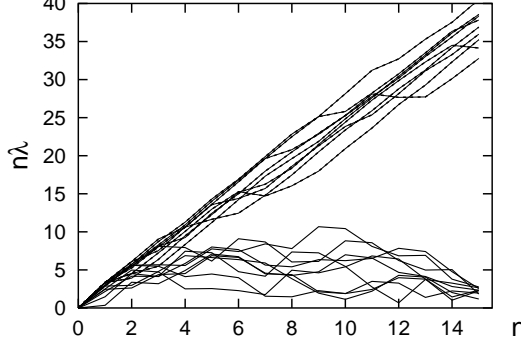


FIG. 4: $n\lambda$ versus n for kicked rotator with $K = 20$. Examples of typical trajectories (slope $\approx \ln(K/2)$, shown dashed), and rare trajectories having $\lambda \leq 1/5$ after 15 iterations (shown by solid lines). Instead of linear increase followed by decrease expected from the simple theoretical model (6-9) the trajectories leading to small values of λ in a real simulation more likely demonstrates a few small oscillations of λn .

narrow features seen in Fig. 2. A function $\lambda(u)$ (10) has a narrow minimum with the depth

$$\lambda_{min} = \lambda_0 |t_1 - t_2|/t, \quad (11)$$

and the width $\delta u = \exp(\lambda_0(|t_1 - t_2| - t - t_2))$. Away from the minimum we may write

$$\lambda = \lambda_0 + (\ln |u| + \lambda_0 t_2)/t \text{ or } |u| = e^{(\lambda - \lambda_0)t - \lambda_0 t_2}. \quad (12)$$

We see that at the time t small values of λ are concentrated in narrow stripes on the x, p plane, each corresponding to the core of a squeezed fold created at an earlier time. Among these lines those created at $t_1 \approx t/2$ have values as small as $\lambda \approx 0$, leading to nonvanishing spectrum at the origin $F(0) > -\infty$. In order to estimate the area in phase space corresponding to $\lambda \ll \lambda_0$, we notice that a fold created at time t_1 had a length ~ 1 . It becomes as long as $e^{\lambda_0 t_2}$ at the time t . This leads to

$$P(\lambda, t) \sim e^{\lambda_0 t_2} du/d\lambda \sim \exp[(\lambda - \lambda_0)t]. \quad (13)$$

In derivation of (13) we ignored fluctuations of Lyapunov exponents during the squeezing stages (6) and (8). Due to fluctuations $P(\lambda, t)$ is saturated by only exponentially small fraction of strongest folds. In our mechanism (6-9) for the trajectory $x(\tau)$, $p(\tau)$ having small λ at $\tau = t$, a value of $\lambda\tau$ should first increase linearly (being $\sim \lambda_0\tau$ for $\tau < t/2$) and then decrease with the same slope. Such a behavior is expected for the trajectory from the core of the typical fold. Fig. 4 shows that this straight scenario should be modified for the trajectories leading most probably to the small values of λ . Still we may say that the simple folding mechanism described by the eqs. (6-9) is sufficient for having a finite value of the spectrum at the origin $F(0) > -\infty$. It is also capable to prevent the probability from decaying at small λ faster than $P(\lambda, t) \propto e^{\lambda t}$. Thus we may write

$$F(0) = -\tilde{\lambda} \gtrsim -\lambda_0, \quad F'(0) \leq 1. \quad (14)$$

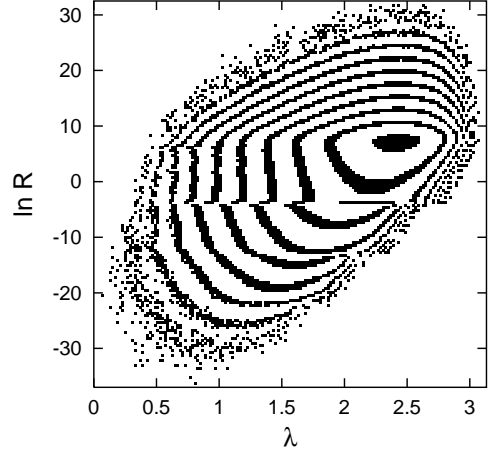


FIG. 5: The contour plot of the joint distribution $W(\lambda, \ln R)$ of the Lyapunov exponent and the logarithm of curvature, Eq. (19), for the kicked rotator with $K = 20$ after 15 iterations. Contours were drawn by taking 10^{12} initial conditions and allocating the results into the bins of two-dimensional histogram. The number of counts increases by 10 for each black contour, from outer to inner (the probability on the inner border of the contour is twice the probability on the outer side). The correlation between small λ and small R confirms our phase-space-folding induced mechanism.

Numerical simulations of Fig. 1 however, are consistent with $F'(0) \approx 1$. The reason for this robustness may be that an exponential $\propto e^{\lambda t}$ increase of probability (13) follows from $|u| \propto e^{\lambda t}$ at the wings of minima of $\lambda(u)$, Eq. (12). Fluctuations of λ_0 in (12) may change the prefactor in the probability, but not its dependence on λ . Even in this form our result has a strong predictive power. One immediately finds from (14) for $m > 0$

$$t^{-1} \lim_{t \rightarrow \infty} \ln \langle e^{-m\lambda t} \rangle = -\tilde{\lambda}. \quad (15)$$

All moments are saturated by rare trajectories with $e^{-\lambda t} \sim 1$ (more precisely, around such a trajectory $\ln |\delta x(t)/\delta x(0)|$ increases with time slower than t^1). An exponentially small value of the average $\langle e^{-m\lambda t} \rangle$ is due to a small number of such the most important trajectories. Eq. (15) should be compared with the often used Gaussian approximation $t^{-1} \ln \langle e^{-m\lambda t} \rangle_G \approx -m(\lambda_0 - m\lambda_2/2)$.

In order to better understand a relation between folding and the value of the Lyapunov exponent we need to introduce a qualitative characteristic of folding, such as the radius of curvature of small bended areas. To this end we first have to describe a nonlinear divergency of the close trajectories. This can be done by expanding the map (4) to the second order in the displacement between trajectories. If we write two components of the displacement $\delta p, \delta x$ as a column \mathbf{q} , then

$$\mathbf{q}_n = \mathcal{M}_n \mathbf{q}_0 + \frac{1}{2} \begin{pmatrix} 1 \\ 0 \end{pmatrix} \mathbf{q}_0^T \mathcal{A}_n \mathbf{q}_0 + \frac{1}{2} \begin{pmatrix} 0 \\ 1 \end{pmatrix} \mathbf{q}_0^T \mathcal{B}_n \mathbf{q}_0, \quad (16)$$

where $\mathcal{M}_n, \mathcal{A}_n, \mathcal{B}_n$ are 2×2 matrices. The monodromy

matrix for kicked rotator is given by a product

$$\mathcal{M}_n = \prod_{i < n} \begin{pmatrix} 1 & K \cos x_i \\ 1 & 1 + K \cos x_i \end{pmatrix}. \quad (17)$$

Two other symmetric matrices may be found from the recursion relations [12].

$$\begin{aligned} \mathcal{A}_{n+1} &= \mathcal{A}_n + (1 + K \cos x_n) \mathcal{B}_n - K \sin x_n \mathcal{C}_n, \\ \mathcal{B}_{n+1} &= \mathcal{A}_{n+1} + \mathcal{B}_n, \end{aligned} \quad (18)$$

where $\mathcal{A}_1 = \mathcal{B}_1 = 0$ and the elements of the matrix \mathcal{C}_n are $(\mathcal{C}_n)_{ij} = (\mathcal{M}_n)_{i2}(\mathcal{M}_n)_{j2}$. Consider as a measure of bending the radius of curvature R_x of the image of a line $\mathbf{q}_0^T \equiv (0, \delta x)$. A simple calculation gives

$$\frac{1}{R_x} = \frac{(\mathcal{A}_n)_{22}(\mathcal{M}_n)_{22} - (\mathcal{B}_n)_{22}(\mathcal{M}_n)_{12}}{((\mathcal{M}_n)_{12}^2 + (\mathcal{M}_n)_{22}^2)^{3/2}}. \quad (19)$$

Similar results may be obtained for R_p^{-1} , the curvature of the image of line $\mathbf{q}_0 \equiv (\delta p, 0)$. The joint distribution $W(\lambda, \ln R_x)$ is shown in Fig. 5. We see that for given λ the curvature may vary by orders of magnitude. However the general trend is transparent: the smaller values of λ correspond to the smaller radius R [13].

We do not investigate here the shape of the right wing of spectrum $F(\lambda)$. For closed conservative systems and periodic maps the shortest unstable periodic orbit sets the exact upper limit for λ . The case of time dependent random potential was considered in Ref. [5].

In conclusion, we have shown that the correlations of the rate of divergency for close families of trajectories have crucial influence on the distribution of Lyapunov exponents. Folding of the phase plane inevitably leads to creation of elongated areas on the plane, where initially diverging trajectories revert to approaching to each other again. This allowed us to claim the existence of the finite limit for spectrum of Lyapunov exponent at the origin $F(0)$ and to estimate the slope $F'(0)$, Eq. (14). Consequently, we found a universal description for all negative moments of the distribution of λ , Eq. (15). To investigate directly a relation between folding and the divergency of trajectories we introduced the joint distribution $W(\lambda, \ln R)$ of the Lyapunov exponent and the logarithm of the curvature of the banded phase space (Fig. 5).

One immediate application of our findings will be a calculation of the Loschmidt echo [14], which was shown [15] to decay on average like $\langle e^{-\lambda t} \rangle$. Another related problem of current interest is finding of the gap in the spectrum of the smooth Andreev billiard. Recently, the similar results were found there within the semiclassical calculation [8], weak disorder averaging [9] and the effective RMT [8, 10]. Taking into account fluctuations of the Lyapunov exponents should further lower the gap.

Discussions with C. W. J. Beenakker, A. N. Morozov and J. Tworzydło are greatly appreciated. This work was supported by the Dutch Science Foundation NWO/FOM.

[1] B.V. Chirikov, Phys. Rep. **52**, 264 (1979).
[2] E. Ott, *Chaos in Dynamical Systems* (Cambridge University Press, Cambridge, 1993).
[3] P. Grassberger, R. Badii, and A. Politi, J. Stat. Phys. **51**, 135 (1988); M. A. Sepúlveda, R. Badii, and E. Pollak, Phys. Rev. Lett. **63**, 1226 (1989).
[4] H. Fujisaka, Prog. Theor. Phys. **70**, 1264 (1983); P. Grassberger and I. Procaccia, Physica D **13**, 34 (1984); R. Badii and A. Politi, Phys. Rev. A **35**, 1288 (1987); T. Tél, Phys. Rev. A **36**, 2507 (1987); S. Vaienti, J. Stat. Phys. **56**, 403 (1989); F. J. Romeiras *et. al.*, Phys. Rev. A **41**, 784 (1990); B. Eckhardt and D. Yao, Physica D **65**, 100 (1993); C. Amitrano and R. S. Berry, Phys. Rev. E **47**, 3158 (1993); M. H. Ernst *et. al.*, Phys. Rev. Lett. **74**, 4416 (1995); A. Adrover and M. Giona, Physica A **253**, 143 (1998); A. Prasad and R. Ramaswamy, Phys. Rev. E **60**, 2761 (1999); F. K. Diakonos *et. al.*, Phys. Rev. E **62**, 4413 (2000); H. Yamada and T. Okabe, Phys. Rev. E **63**, 026203 (2001).
[5] H. Schomerus and M. Titov, Phys. Rev. E **66**, 066207 (2002).
[6] M. G. Brown, J. A. Colosi, S. Tomsovic, A. Virovlyansky, M. A. Wolfson, and G. M. Zaslavsky, J. Acoust. Soc. Am. **113**, 2533 (2003).
[7] M. A. Topinka *et. al.*, Nature **410**, 183 (2001).
[8] P. G. Silvestrov, M. C. Goorden, and C. W. J. Beenakker, Phys. Rev. Lett. **90**, 116801 (2003).
[9] M. G. Vavilov and A. I. Larkin, Phys. Rev. B **67**, 115335 (2003).
[10] C. W. J. Beenakker, cond-mat/0406018.
[11] The matrix \mathcal{M} may be decomposed as $\mathcal{M} = \mathcal{U}\mathcal{T}$, where a real symmetric matrix \mathcal{T} ($\det \mathcal{T} \equiv 1$) describe squeezing and stretching with respect to some normal axes, and a normal matrix \mathcal{U} describes the rotation of the plane. We define λ (3) through the eigenvalue of $\mathcal{M}^T \mathcal{M} = \mathcal{T}^T \mathcal{T}$.
[12] Solutions of eqs. (17,18) at each time step n comply with the conditions, imposed by the area conservation: $\det \mathcal{M} \equiv 1$, $\mathcal{M}_{11}\mathcal{B}_{11} + \mathcal{M}_{22}\mathcal{A}_{12} - \mathcal{M}_{12}\mathcal{B}_{12} - \mathcal{M}_{21}\mathcal{A}_{11} \equiv 0$, and $\mathcal{M}_{11}\mathcal{B}_{12} + \mathcal{M}_{22}\mathcal{A}_{22} - \mathcal{M}_{12}\mathcal{B}_{22} - \mathcal{M}_{21}\mathcal{A}_{12} \equiv 0$.
[13] For kicked rotator with $K \gg 1$ the distribution of R has a main peak at $R \sim K^2$ and a small narrow peak at $R \sim 1/K$, both seen at Fig. 5. In Fig 2 these peaks correspond to the straight and the curved segments respectively.
[14] R. A. Jalabert and H. M. Pastawski, Phys. Rev. Lett. **86**, 2490 (2001).
[15] P. G. Silvestrov, J. Tworzydło, and C. W. J. Beenakker, Phys. Rev. E **67**, 025204(R) (2003).